33RD CONGRESS
OF THE INTERNATIONAL COUNCIL
OF THE AERONAUTICAL SCIENCES
STOCKHOLM, SWEDEN, 4-9 SEPTEMBER, 2022

ICAS 2022 SWEDEN

THERMODYNAMIC POTENTIAL OF TURBOFAN ENGINES WITH DIRECT COMBUSTION OF HYDROGEN

Alexander Görtz[1] & Daniel Silberhorn[2]

[1]German Aerospace Center, Institute of Propulsion Technology, Cologne, Germany, Alexander.Goertz@dlr.de
[2]German Aerospace Center, Institute of System Architectures in Aeronautics, Hamburg, Germany, Daniel.Silberhorn@dlr.de

Abstract

Over the last decades passenger numbers in aviation have been increasing exponentially. This results in a higher climate impact due to emissions but this effect can be reduced by using carbon dioxide neutral fuels. The change to hydrogen as a fuel is a promising step towards climate neutral aviation. This change leads to new questions regarding gas turbine engines, aircraft design and the overall energy sector. In particular, the influence and potential on the engine is still unclear as the hydrogen is stored in liquid form at 20 K. Furthermore, its combustion process is different to kerosene and the exhaust gas has different properties. For this reason, two short range aircraft have been designed for the entry into service 2040, first a conventional aircraft and a second variant using hydrogen as fuel. The thrust requirements created are used to design new turbofan engines on a thermodynamic level. Additionally, for the hydrogen case three concepts of conditioning have been investigated. The change to hydrogen is expected to improve the specific fuel consumption up to 4.6 %. Intercooling as conditioning concept proves to be the best thermodynamic solution but also leads to the largest heat transfer surface. In addition, boundary conditions for the heat exchanger design of the three concepts are presented.

Keywords: Hydrogen, Turbofan, Aero Engine, Heat Exchanger, Aviation

1. Introduction

Passenger numbers in aviation are increasing exponentially for years. This growth was currently interrupted in 2020 by the COVID pandemic which led to a sudden decrease in passenger numbers by 50 % in the period from 2019 to 2020 [1]. Nevertheless, it can be expected that the passenger numbers will reach the value of 2020 again within a short period of time. 5 % of the human impact on climate change is due to aviation and this percentage increases when the numbers of passengers are growing [2]. Among the emissions, especially carbon dioxide, water vapor and nitrogen oxides have a large influence on climate change. The European commission has set high goals to reduce the climate impact of aviation: For the year 2050, the goal is a reduction of 75 % for the carbon dioxide emissions and a reduction of 90 % for nitrogen oxide emissions [3]. These numbers are relative to a typical new aircraft in 2000.

Evolutionary development like modern geared turbo fans [4], new materials [5] and further improvement of existing technologies are still a reasonable way forward but the impact of this path will become smaller with each iteration. To reach the defined objectives, revolutionary propulsion concepts have to be considered. The opportunity of electric propulsion with batteries or fuel cells is probably only feasible for the urban mobility or short-range application [6]. Due to the much higher power density of gas turbines, these will remain the technology of future propulsion [7]. In order to reach the climate goals, it is urgently necessary to step away from fossil fuels to a sustainable solution. This could be achieved by either switching to sustainable aviation fuels (SAF) or to hydrogen. Both possibilities imply a major change in the infrastructure not only for the airport but for the whole energy sector [8].

The usage of hydrogen also involves new engineering solutions on aircraft and engine level which is mainly due to the hydrogen's low density, its combustion properties and its low storage temperature. Hydrogen has to be stored in its liquid state (LH2) at around 2 bar and 20 K but should be burned at a much higher temperature and pressure [9] [10]. The energy sector has always been looking for alternative energy carriers besides oil and gas. Hydrogen is seen as a potential fuel since 1918 [11]. In the early 2000s, the European Commission started the Cyoplane project [12] [13]. The goal was to analyze hydrogen fueled aircraft using an approach of minimal change. This project concluded that the energy consumption for this application would increase by 9 - 14 %. Other work predict a decrease in fuel consumption [14] [10]. With simultaneous adaptation of the aircraft, Vearstrate discovered a potential to reduce the energy utilization of long range transport aircraft by approximately 11 % [15]. Because of the new fuel tank specifications and the changed aircraft mass distribution as a consequence, the thrust requirements for a hydrogen combustion engine differ from the requirements of a conventional kerosene burning aero engine. This leads not only to other internal temperatures and rotational speeds but also to the necessary installation of a heat exchanger for the liquid hydrogen. It is not yet clear where the needed heat for this process will come from but three possible locations are evaluated. Exhaust cooling (EC), Inter Compressor Cooling (ICC) and Cooled Cooling Air (CCA) are the concepts of interest.

2. Thermodynamic Properties of Hydrogen

Hydrogen as a fuel is fundamentally different from conventional kerosene and must therefore be treated differently both in the engine and in the entire aircraft. The most striking aspect here is the density and the energy density. Liquid hydrogen contains 2.8 times more energy than kerosene per kilogram fuel but needs a volume 4 times bigger to store this amount of energy [13]. The higher energy density of hydrogen is represented by the lower heating value (LHV). While the LHV of kerosene is $LHV_{Kerosene} = 43.25\,MJ/kg$ [16], that of hydrogen is $LHV_{H2} = 119.9\,MJ/kg$ [17]. Another important point regarding the combustion is the adiabatic combustion temperature which can be seen in figure 1. For both kerosene and hydrogen this temperature is shown over the equivalent ratio Φ. At a value of $\Phi = 1$ the maximum combustion temperature is reached and is around 3.5 % higher for hydrogen.

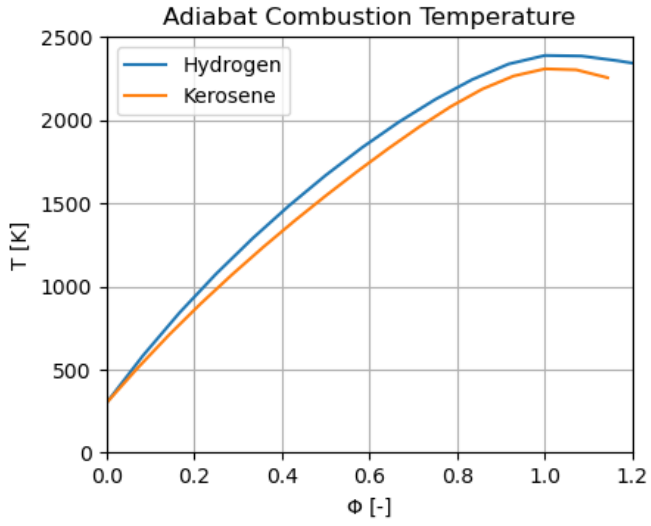

Figure 1 – Adiabat Combustion Temperature at standard atmospheric conditions

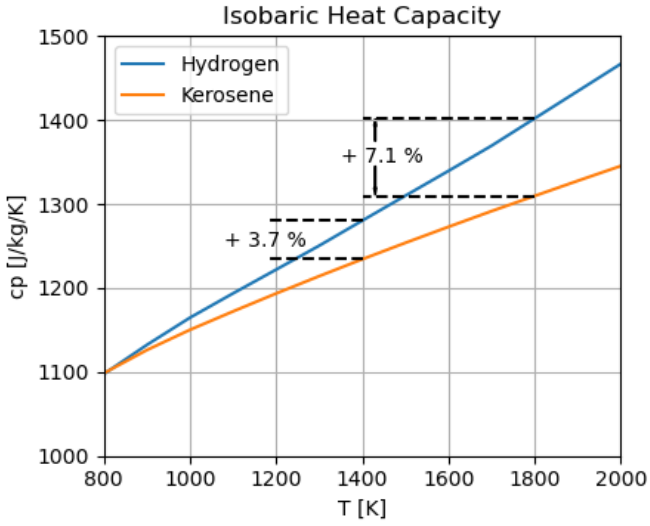

Figure 2 – Heat Capacity After Combustion for 800 K mixture temperature

Another important property is the heat capacity of the exhaust gas after combustion with air in figure 2. This diagram shows the isobaric heat capacity after a combustion for different temperatures. Here, each point has a different fuel to air ratio (FAR) to achieve the temperature on the x-axis. Each mixture starts with a temperature before combustion of 800 K. For a typical range of burner outlet temperatures, from 1400 K - 1800 K, the hydrogen exhaust gas has a increased heat capacity from

3.7 % - 7.1 %. This increase is due to the higher content of water in the exhaust flow, since water has a much higher heat capacity than air. For the same amount of energy added with combustion, the hydrogen exhaust has a by 2.5 % higher water content than the kerosene exhaust gas [13]. Furthermore, the evaporation temperature of liquid hydrogen is slightly above 20 K at atmospheric pressure [18] which also leads to very high requirements for the tank system. The hydrogen will be stored in its liquid form but it has to be burned in its gaseous form. This evaporation process is shown in simplified form in the T-s diagram figure 3. Assuming evaporation at constant pressure above the critical pressure $p_{crit} = 13.15\,bar$, the hydrogen does not pass through the two-phase region. Within a gas turbine application, the evaporation of the hydrogen is done supercritically since the operating pressures are higher than the critical pressure.

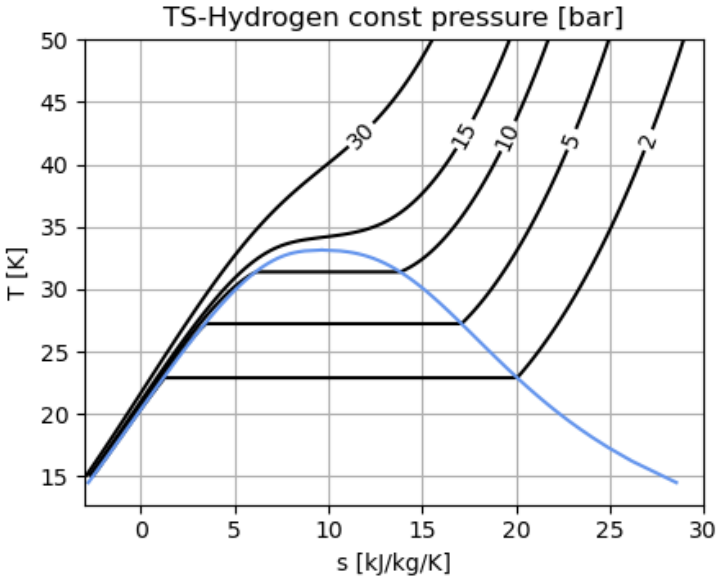

Figure 3 – Hydrogen T-s-Diagram with constant pressure lines

3. Methods

The methods used to calculate the following data are described in this section. The main applied methods are the thermodynamic cycle calculation for the engine, the overall aircraft design and the heat exchanger operating behavior. All methods were used to design engines appropriate for the corresponding flight mission.

3.1 Engine Performance

To design the thermodynamic cycle, a conceptual approach was selected using the performance program (DLRp2) within the virtual propulsion system framework Gas Turbine Laboratory (GTlab) [19] [20]. GTlab is being developed at the Institute of Propulsion Technology of the German Aerospace Center and is used for multidisciplinary simulations of gas turbines at different levels of detail [21]. To rate the designed engines in this paper, a reference gas turbine is set up based on the General Electric CF6 engine. The reference engine is a geared turbo fan (GTF) designed for an entry into service (EIS) 2040 and powered by standard kerosene. In order to be able to evaluate the potential of hydrogen combustion, new engines will subsequently be designed for hydrogen application. The conditioning of the liquid hydrogen is taken into account and the methods used to calculate the heat exchanger can be found in Chapter 3.3

3.2 Aircraft Design

To provide the overall aircraft performance including the thrust requirements for the turbofan engine design, disciplinary tools are integrated into a workflow which is build in RCE [22]. To allow seamless communication between the disciplines, the data schema CPACS [23] [24] is applied. It also allows

data transfer between the high fidelity engine design and the overall aircraft environment. The core aircraft sizing tool within the workflow is openAD [25]. It provides the initialization and the synthesis of the aircraft concept. Furthermore, the low-speed and high-speed performance tools LSperfo [26] and AMC [27] are integrated. They combine the aerodynamic and propulsion performance which is provided in form of performance decks. Furthermore, mass related inputs together with mission definitions are needed. This propulsion performance deck is the interface between the overall aircraft design and the engine design, allowing a clean data transfer within the whole envelope.
Since the liquid hydrogen (LH2) storage and distribution is the most challenging part of LH2 powered aircraft, advanced methods are applied including a dynamical thermodynamic calculation of the tank behaviour along the trajectories. A more detailed description of LH2 tank design methods can be found in Burschky [28]. Correlations by Brewer [10] are applied to estimate the mass of the storage subsystems as well as the distribution system.
For calibration and validation purposes, the Boeing 767-300 [29] is recalculated and the top level aircraft requirements (TLAR) are derived, see Table 1. The derived concepts for the entry into service (EIS) of 2040 incorporate advanced turbofan engines and carbon fibre reinforced polymer wing structure. Furthermore, the wing span is increased to 52 m to match the ICAO Aerodrome Reference Code D which strongly decreases the lift induced drag.

	Unit	**Value**
Design Range	NM	3900
Desing PAX (two class)	-	261
Design Payload	kg	261000
Cruise Mach number	-	0.8
TOFL (ISA SL)	m	2400
Approach Speed (MLM)	kt	140
Wing Span Limit	m	52

Table 1 – Top Level Aircraft Requirements

3.3 Heat Exchanger

Since the use of a heat exchanger for hydrogen in an engine context is new, the method for calculating is explained in more detail here. The used method is called NTU-Method [30] (Number of Transfer Units) and is used for all conditioning concepts EC, ICC and CCA. The method is well known and widely used in industry and science [31] [32]. It is also being applied for research into the use of heat exchangers in commercial turbojet engines and therefore in aviation overall [33]. Furthermore, this method is also used for hydrogen application, e.g. for refueling hydrogen stations [34]. Within a turbofan engine, hydrogen will flow on one side of the heat exchanger and air will flow on the other. Depending on the respective concept, the air is either dry air or air with combustion gases. The NTU method is used either to design new heat exchangers or to calculate existing ones with different inlet conditions. This procedure simplifies the design considerably, as it saves complicated calculations of flow forms and local heat transfers.
In general, the inlet conditions of both fluid streams, mass flow $\dot{m}_i$ and temperature T_{iE}, are known and therefore the heat capacity c_{pi} can be calculated. During the design process the overall geometry is unknown but an additional value is given. This can be either the transferred heat $\dot{Q}$ or the outlet temperature T_{iA} of one side. Thus, equations 1a and 1b are completely defined and determinable.

$$\dot{Q} = \dot{m}_1 \cdot c_{p1} \cdot (T_{1E} - T_{1A}) = \dot{W}_1 \cdot (T_{1E} - T_{1A}) \tag{1a}$$

$$\dot{Q} = \dot{m}_2 \cdot c_{p2} \cdot (T_{2A} - T_{2E}) = \dot{W}_2 \cdot (T_{2A} - T_{2E}) \tag{1b}$$

While all temperatures are known, the dimensionless temperature change P_i can be determined using equation 2. This value describes the temperature change of one side i in relation to the largest temperature difference occurring in the heat exchanger.

$$P_1 = \frac{T_{1E} - T_{1A}}{T_{1E} - T_{2E}}; \quad P_2 = \frac{T_{2A} - T_{2E}}{T_{1E} - T_{2E}} \tag{2}$$

For further calculations, the ratio of heat capacity flows $\dot{W}_i$ is needed, equation 3. This differs from the ratio of mass flows, especially when there are different fluids on both sides.

$$R_1 = \frac{\dot{W}_1}{\dot{W}_2}; \quad R_2 = \frac{\dot{W}_2}{\dot{W}_1} \tag{3}$$

The value P_i can additionally be determined in another way. For this, P_i is represented as a function of NTU_i and R_i. This dependency can be seen in equation 4. Note that this equation is only valid for a counter flow configuration. For other types of heat exchangers, the corresponding formulas can be found in [30].

$$P_i = \frac{1 - exp[(R_i - 1) \cdot NTU_i]}{1 - R_1 \cdot exp[(R_i - 1) \cdot NTU_i]} \tag{4}$$

Rearranging equation 4 leads to a $NTU_i = f(P_i, R_i)$ in equation 5.

$$NTU_i = ln\left(\frac{1 - P_i}{1 - P_i \cdot R_i}\right) \cdot \frac{1}{R_i - 1} \tag{5}$$

Hence, a relation between NTU_i, $\dot{W}_i$, k and A can be defined, see equation 6. Here A represents the heat transfer surface and k the overall heat transfer coefficient.

$$NTU_1 = \frac{kA}{\dot{W}_1}; \quad NTU_2 = \frac{kA}{\dot{W}_2} \tag{6}$$

This NTU method can be charted and the operating behavior can also be evaluated on a graphic level. An example of the charts can be found in figure 8.
During the design process, this method is straight forward. There is no geometry yet available and therefore the surface area and the heat transfer coefficient are results. This changes for an off design calculation where the input conditions and the surface are given. The off design behavior can either be solved graphically or iterative via equations 1a - 6. Both approaches assume an estimated kA_{target}. The iterative procedure, which was chosen in this work, guesses the transferred heat $\dot{Q}_{guess}$ and a new kA_{new} can be determined. If the difference $kA_{target} - kA_{new}$ is smaller than a threshold, the iterative process is assumed to be converged.

4. Aircraft

The designed aircraft concepts powered with kerosene and liquid hydrogen are shown in Figure 4. The LH2 concept incorporates two storage tanks in front and behind the cabin which are insulated with spray-on foam. At 2000 NM, the kerosene baseline reduces the block energy by 39% compared with the B767 similar reference. The LH2 powered concept has a slightly increased design block energy consumption of 3% compared to the synthetic kerosene baseline. Further details of these concepts together with their climate impact assessment are described in [35]
The thrust requirements of 5 representative flight conditions are derived from the overall aircraft design methodologies and shown in Table 2 for the kerosene and LH2 powered baselines, respectively. The cruise and Top of Climb (TOC) high-speed thrust requirements are higher for the LH2 concept. This is because of the increased fuselage width and length to accommodate the big LH2 storage tanks which leads to reduced aerodynamic performance due to the increased wetted area. The reduced take-off thrust of the LH2 concept results from the lower wing-loading at maximum take-off mass (MTOM) condition which allows to rotate and lift-off at lower speeds. This reduced wing-loading results from the reduced overall lower fuel mass for LH2 due to the higher heating value. That means, the difference between MLM and MTOM is much lower for the LH2 case. Since both concepts are designed for the approach speed of 140 kn calibrated airspeed at MLM, the wing loading at MLM of both concepts is rather similar.

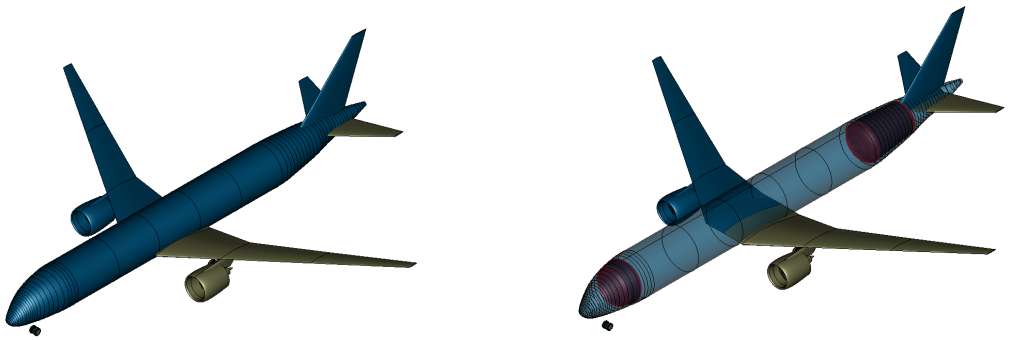

(a) (b)

Figure 4 – Isometric view of 2040 Kerosene (a) and LH2 concept (b).

Rating	Thrust Kerosene [kN]	Thrust Hydrogen [kN]	Mach [-]	Alt [m]	dTISA [K]
Take-off	189.5	168.6	0	0	0
End of field	119.7	126.9	0.24	11	0
2nd Segment	124.3	131.2	0.25	122	0
Top of Climb	33.1	35.9	0.78	10668	10
Cruise	29.3	31.7	0.8	11278	0

Table 2 – Thrust Requirements

5. Engine Model

All engines in this paper have the same baseline architecture which can be seen in the performance model in figure 5. This is a two spooled geared turbofan, designed for an entry into service 2040 and powered by either kerosene or hydrogen. Both the high pressure (HPT) and the low pressure turbines (LPT) are assumed to be cooled. Fan and booster compressor are powered by the LPT while the high pressure compressor (HPC) is powered by the HPT. Furthermore, the engines are unmixed which results in two separate and consequently independent nozzles. In addition, a power off take from the high pressure shaft and a bleed off take is considered. This architecture is enhanced for the hydrogen cases with a heat exchanger providing the necessary energy to evaporate the liquid fuel. The position of this heat exchanger varies with the respective conditioning concept. For each concepts EC, ICC and CCA this position can also be found in figure 5. The thrust requirements needed to design the engines are presented in section 4.

The engines were designed for cruise flight using the following assumptions regarding the performance calculation. The fan diameter is one of the mayor design variables in this work and is set to a value of $D_{Fan} = 2.7m$. This can be seen as the technological challenge for this class of aircraft because the engine might not fit under the wing of the aircraft. Since there was no iterative design of the overall aircraft and the engine regarding the fan diameter, this diameter was set to a fixed value for all engines. Due to the separate nozzles for the core and the bypass, the fan pressure ratio can be adjusted to achieve an ideal speed ratio of the nozzles in cruise flight [36]. In addition, a constant ratio of the fan bypass to core pressure ratio of 0.9 is assumed. The fans gear ratio is calculated by setting the fans tip speed to a mach number of 1.1 while the low pressure shafts rotational speed is set by a maximum loading of the LPT to $AN^2_{LPT} = 12000\frac{m^2}{s^2}$ which occurs at the top of climb. If not mentioned differently, the boosters pressure ratio is set to 20 % of the HPCs pressure ratio. For simplicity, component efficiencies are held constant throughout the design process for all engines. As is usual in cycle calculation, scaled maps are used to represent the operating behavior of the turbo components aside from the design point.

Since the thrust requirements differ significantly between the kerosene and hydrogen aircraft, the

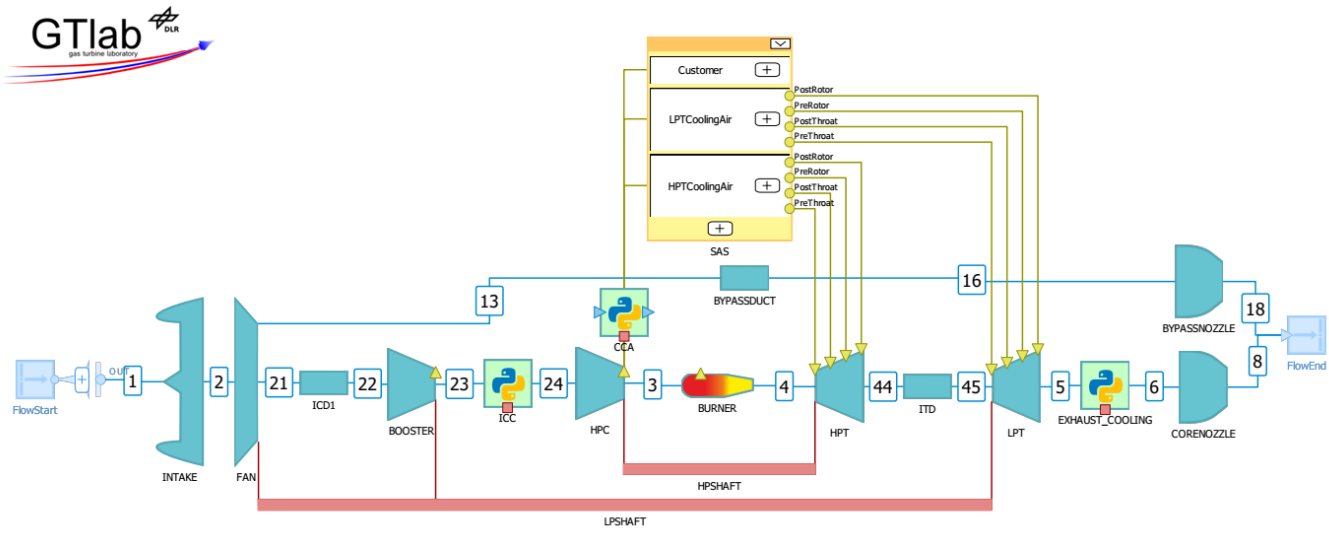

Figure 5 – Engine model for all architectures

following sections explain assumptions and calculation procedures that change specifically for each fuel.

5.1 Kerosene Engine Specifics

The operating point with the highest loading and therefore the highest appearing temperatures is maximum take off at $TISA + 15\,K$. This operating points determines the temperature limits during the engines design process. For the compressor outlet temperature, this limit was set to $T_{3,max} = 950\,K$. Thus, the overall pressure ratio of the engine is also set by this value. The maximum turbine entry temperature is reached as well at maximum take off and is set to $T_{4,max} = 1950\,K$. By limiting temperatures at an operating point aside from the design point, the temperatures and the OPR are indirectly given in cruise flight. Furthermore, the demand for cooling air at the HPT is also determined at maximum take off since the highest temperatures define the amount of cooling air needed. This mass flow of air is calculated by using diagrams from [37] which contain the cooling air temperature and the temperature after the first stator of the turbine. The amount of cooling air for the LPT is set to a constant value of 2.5 % of the compressor inlet mass flow.

5.2 Hydrogen Engine Specifics

Due to the lower thrust requirements for take off, it is unclear which operating point sets the temperature limits for T_3 and T_4. Using the same method from the kerosene engine as in chapter 5.1 would result in much higher temperatures in cruise. It is uncertain if the materials can resist such high temperatures for a large amount of time. The same argumentation applies also to the demand of cooling air because take off might not be setting the required cooling air mass flow. To handle this fact, a temperature limit for cruise was introduced so that $T_{3,curise,kerosene} = T_{3,curise,hydrogen}$ and $T_{4,curise,kerosene} = T_{4,curise,hydrogen}$. Furthermore, the amount of cooling air for the hydrogen engine is set to the same value as for the kerosene engine. Only for the CCA concept, a conservative calculation using [37] is included because the main goal of CCA is to reduce the cooling air.

A few further assumptions for the heat exchanger were used in the performance calculation. The liquid hydrogen is stored in a tank within the fuselage of the aircraft at a temperature of 20 K and has to be transported to the engine itself. It is assumed that by the time the liquid hydrogen reaches the engine, it still has a temperature of 20 K. This is the same temperature for all operating points. To ensure a reasonable injection of the fuel, its pressure is increased so that it is 5 bar above the pressure of the core flow at the entry to the combustion chamber. The fuel temperature at injection should be between 150 K and 250 K [38] which is the outlet temperature of the heat exchanger. For the design point, this value is set to $T_{Fuel} = 250\,K$ and defines the overall heat transfer in equation

1b and thereby the heat exchanger itself. For the off design calculation the kA_{Target} from chapter 3.3 is set constant to kA_{Design}. Furthermore, constant pressure losses for both heat exchanger sides are assumed.

6. Results

In this section, results for the thermodynamic analysis of the turbofan engines and for the heat exchangers are presented. A distinction is made between the three conditioning concepts EC, ICC and CCA. If not mentioned differently, all data belong to cruise flight.

6.1 Overall Engine

Prior to setting all boundary conditions and specifications to the final engines, parameter studies of the main design values have been executed. At this point, the influence of the respective design value on the engine and on the potential of switching fuels was of interest. The presented studies in this section show the engines increase in efficiency by means of the thrust specific energy consumption (TSEC) while switching from kerosene to hydrogen. As the density and the lower heating value of hydrogen differs from kerosene, it is unfavorable to validate the commonly used thrust specific fuel consumption (TSFC) as a metric. For this value, the thrust is set in relation to the energy required and not to the required fuel mass flow. Furthermore, the studies show the influence of the selected parameter on the heat exchangers size. The value kA is utilized for this because it can be used as a qualitative measure for its size. For each of the studies conducted in this way, the design method presented in Chapter 5 was used. For the sake of overview, only a selection of the studies is shown here.

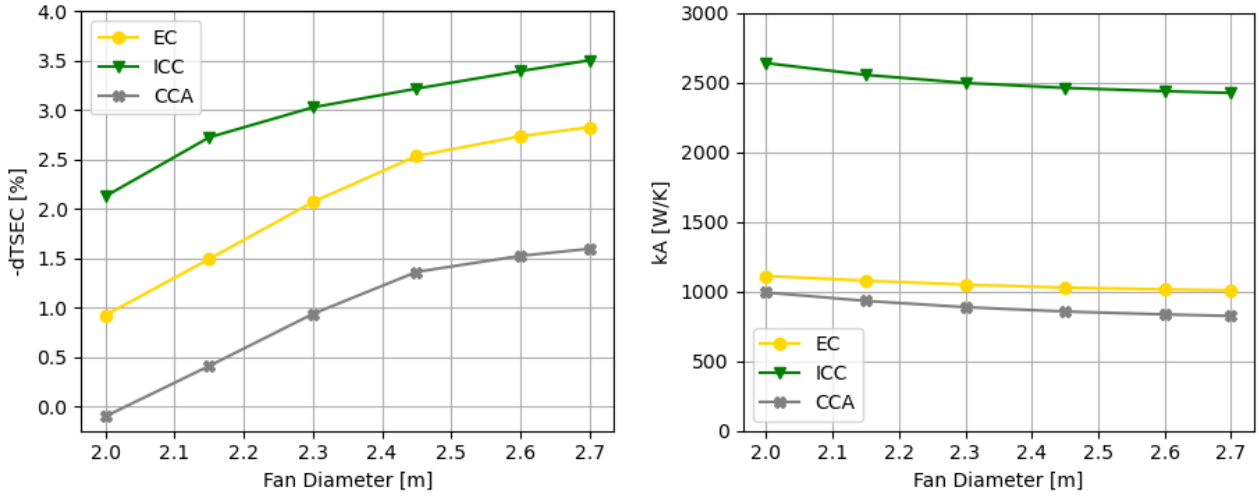

(a) Relative Improvement

(b) Heat Transfer Capability

Figure 6 – Fan Diameter Study

A variation of the fan diameter D_{Fan} between 2.0 m - 2.7 m is shown in figure 6. The increase in efficiency or decrease of TSEC is due to the fact that the exhaust gas has a higher specific heat capacity after combustion with hydrogen, as already shown in chapter 2. Regarding this reduction in TSEC, all three concepts follow the same trend by an increasing difference in TSEC between the fuels. This means that an engine with a higher diameter benefits more from the fuel switch. It should be noted here that the turbine inlet temperature also increases for a larger fan diameter. This is because the inlet temperature into the turbine is limited during the take off flight. If the diameter is increased, the bypass ratio of the engine also increases. However, a high bypass ratio also results in a higher turbine entry temperatures at cruise flight by a given take off turbine temperature. The higher the temperature in cruise flight, the higher the benefit from the heat capacity increase, see chapter 2. What is not visible at this point is the actual improvement of the cycle by increasing the diameter, since only the difference of the engines is shown here. Moving to the second figure (6 (b)),

the size of the heat exchanger becomes qualitatively clear by using heat transfer capability kA. As mentioned above, the bypass ratio increases and the fuel flow decreases with higher fan diameters. Therefore, all mass flows participating in the heat transfer are reduced which results is a smaller heat exchanger. In addition, the overall pressure ratio also increases with a lager diameter. This results in higher exhaust gas temperatures for ICC and a higher inlet cooling air temperature for CCA. The higher temperatures leads to higher temperature differences within the heat exchanger and therefore to better heat transfer. Since the turbine outlet temperature changes barely, the gradient of the curves for ICC and CCA is higher than for EC.

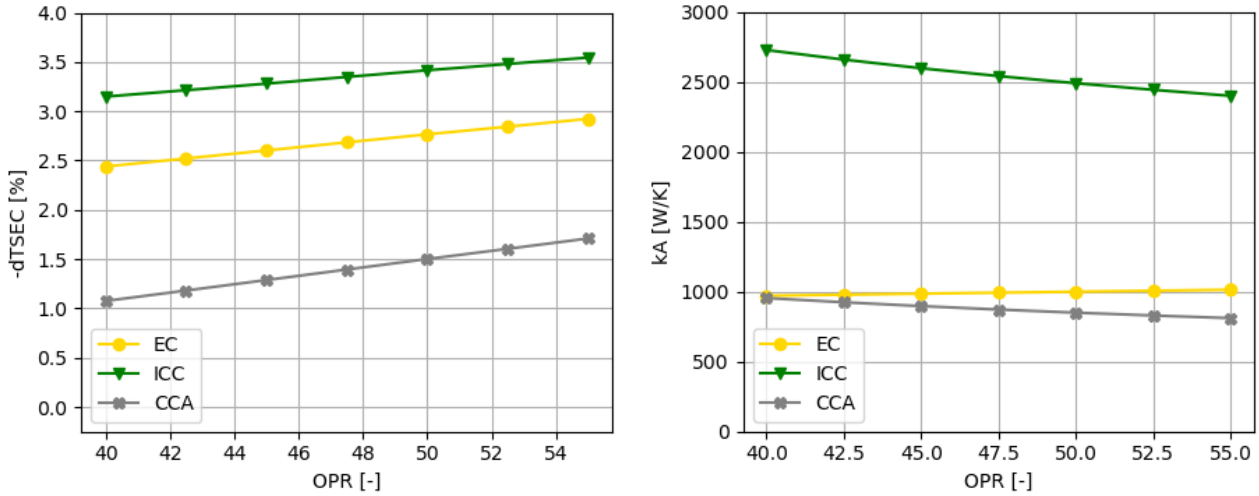

(a) Relative Improvement

(b) Heat Transfer Capability

Figure 7 – OPR Study

The same type of study was also conducted for the overall pressure ratio and can be seen in figure 7. It should be noted that the limit for the compressor outlet temperature was switched off at this point, since otherwise it would not be possible to define the overall pressure ratio. The fan diameter is set to 2.7 m for all engines. The results for this study are similar to the results from the previous calculations. An increase in overall pressure ratio leads to a higher benefit from switching from kerosene to hydrogen. The turbine inlet temperature is basically identical for all engines but the temperature difference across the turbines is higher with increasing overall pressure ratio. This allows more power to be extracted from the mass flow due to the higher heat capacity. Once again, the absolute improvement in TSEC is not noticeable here, but all engines have lower fuel consumption with increasing overall pressure ratio. Analogous to the diameter study is the size of the heat exchanger. The higher pressure and therefore higher temperature at the heat exchanger entry leads to a higher heat transfer. Since this effect does not occur with EC, the size remains fairly constant at this point.

In this case, the greatest possible improvement and the lowest fuel consumption can be achieved with a fan diameter of 2.7 meters and the highest possible compressor outlet temperature or overall pressure ratio. This information is used to design further engines and the results are shown in table 3. In addition to the already known engine types, which are kerosene combustion, EC, ICC and CCA, a further theoretical variant is added to the table. The additional engine is a hydrogen burning variant that has no heat exchanger and where the hydrogen is always supplied gaseous at 250 K. This variant is added to validate whether the heat exchanger improves or worsens the cycle. Since the compressor outlet temperature is limited at the design point, the overall pressure ratio is the same for all engines $OPR = 53.3$ except the ICC type with $OPR_{ICC} = 63.3$. The unique advantage of the ICC concept is that higher overall pressure ratios can be realized, since inter cooling reduces the outlet temperatures of the compressor. A limit for the overall pressure ratio was found by limiting the compressor outlet channel height to a minimum of 12 mm. All engines have a very high and optimistic

bypass ratio of over 18, which is mostly due to the high diameter of the engine. The temperature at compressor outlet is fixed for all cases $T3 = 818\,K$ as described in chapter 5. Only for ICC a different temperature is reached, which can be described with the same reasoning as for the overall pressure ratio. The turbine entry temperature is set to $T4 = 1712\,K$. The amount of cooling air has resulted from the calculation for kerosene and is set to 19 % except for the CCA concept. The goal of cooled cooling air is to reduce the mass flow needed and therefore the same method for cooling air calculation from the kerosene engine was adapted for the CCA type. In general, it can be said that ICC has the greatest potential to improve the cycle with up to -4.6 % regarding the TSEC. In addition, ICC is the only concept that uses the heat exchanger to achieve further improvement. For the other concepts, the engines energy consumption increases by the use of the heat exchanger. However, for the EC and CCA variants, only the improvements become smaller. Globally, all concepts show an increase in energy efficiency compared to kerosene between -1.7 % and -4.6 %. In the case of exhaust gas cooling, the potential decreases because energy is extracted from the exhaust gas, which is no longer available for generating thrust. Intuitively, a high improvement would be expected if the cooling air of an engine is reduced from 19 % to 15.6 %. However, the cooling air has a much lower temperature (see chapter 3.3) and can therefore be used less for power extraction in the following.

	Unit	Kerosene	Hydrogen	EC	ICC	CCA
OPR	-	53.3	53.3	53.3	63.3	53.3
BPR	-	18.47	18.5	18.36	18.9	18.9
$T3$	K	818	818	818	807	818
$T4$	K	1712	1712	1712	1712	1712
$Rel.CoolingAir$	-	0.19	0.19	0.19	0.19	0.156
$\dot{m}_{Fuel}$	kg/s	0.398	0.151	0.152	0.1499	0.154
$TSFC$	g/kNs	13.6	4.77	4.81	4.73	4.87
$TSEC$	W/N	588	567	571	561	578
$dTSEC$	%	0	-3.5	-2.9	-4.6	-1.7

Table 3 – Cruise Engine Performance Data

6.2 Heat Exchanger

Some specific values for the heat exchanger are shown in Table 4. The numbering 1 represents the exhaust gas mass flow and 2 the hydrogen to be vaporized. The transferred heat $\dot{Q}$ is very similar for the three concepts and varies from 481 kW to 499 kW. This is due to the fixed temperature of the hydrogen. Hydrogen always enters the heat exchanger at $T2_{In}$= 20 K and leaves at $T2_{Out}$= 250 K since this is a specification for the design calculation. The inlet temperature of the exhaust gas $T1_{In}$ is significantly depended from the heat exchangers position. The ECs inlet temperature is quite

	Unit	EC	ICC	CCA
$\dot{Q}$	kW	481	484	499
$T1_{In}$	K	643	378	818
$T1_{Out}$	K	621	354	665
$T2_{In}$	K	20	20	20
$T2_{Out}$	K	250	250	250
$p1$	bar	0.325	1.32	17.53
$p2$	bar	23.7	28.1	23.7
$\dot{m}1$	kg/s	19.28	19.64	3.03
$\dot{m}2$	kg/s	0.152	0.1499	0.154
kA	W/K	981	2245	824

Table 4 – Heat Exchanger Cruise Data

high with 643 K since it is positioned directly after the LPT. The heat exchanger of the ICC concept experiences only low temperatures of 378 K and the CCAs has the highest inlet temperature of 818 K. Because the heat transfer is very small compared to the enthalpy flow of the exhaust side 2, the temperature of the exhaust gas changes only slightly across the heat exchanger. Similar to the exhaust gases temperature, its pressure p1 is also given by the heat exchangers position within the engine. The hydrogens pressure is set to 5 bar over the compressor outlet pressure, to ensure a good fuel injection. Therefore, the pressure is directly depended on the overall pressure ratio. This ensures that the evaporation of the hydrogen happens supercritically at any point. The mass flow $\dot{m}2$ corresponds to the fuel mass flow. There is little difference between the heat transfer capability of EC $kA_{EC} = 981\frac{W}{K}$ and CCA $kA_{CCA} = 824\frac{W}{K}$. ICC needs the largest heat exchanger with almost 2.5 times the size of the other heat exchangers $kA_{ICC} = 2245\frac{W}{K}$.

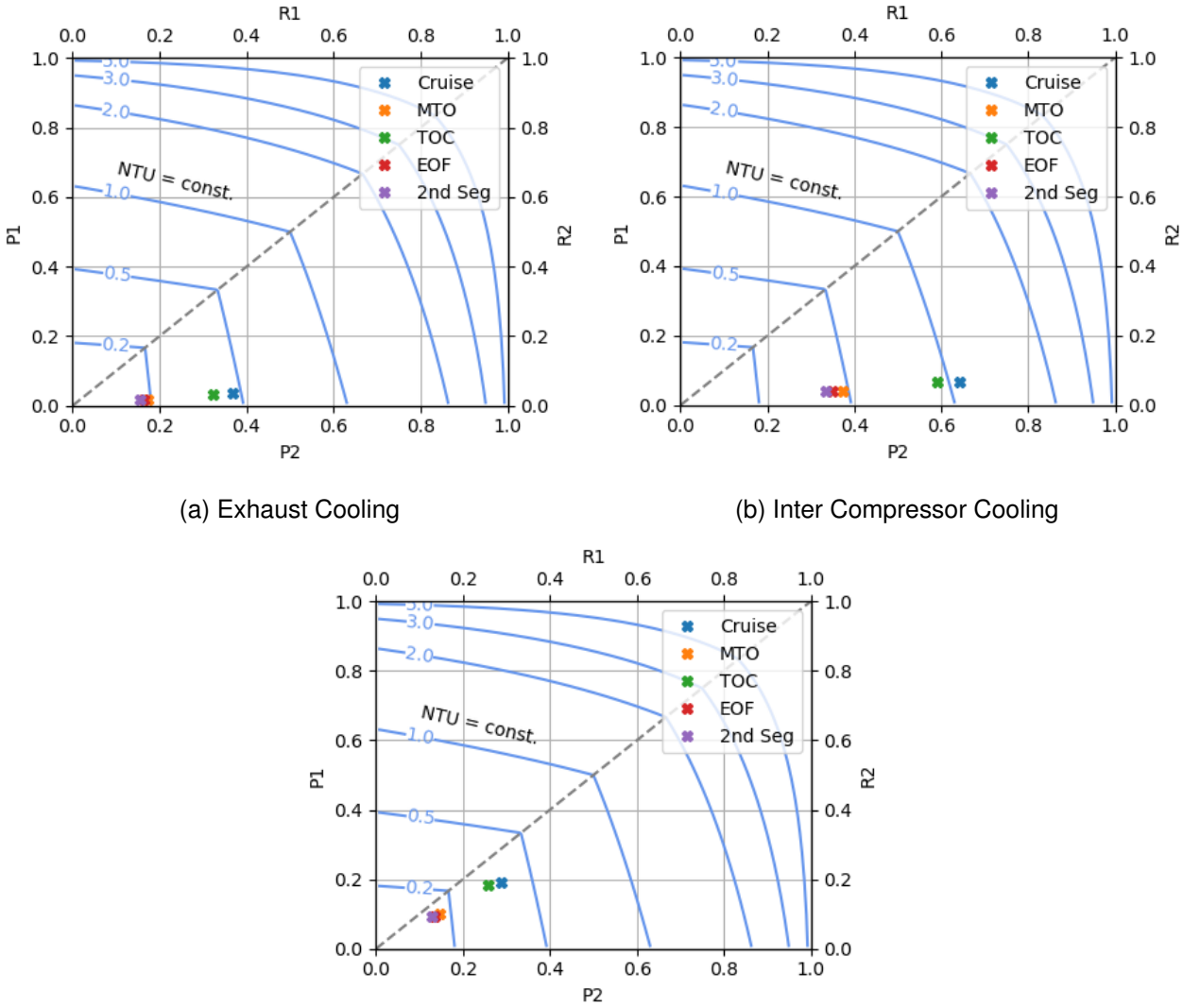

(a) Exhaust Cooling

(b) Inter Compressor Cooling

(c) Cooled Cooling Air

Figure 8 – Heat Exchanger Operating Points

The operating behavior of the heat exchangers is presented in the following figures 8 using the graphical interpretation of the NTU method. The NTU method and the definition of the respective values can be found in chapter 3.3 Each diagram (a) - (c) represents one of the conditioning concepts for liquid hydrogen and includes the operating points given by the thrust requirements table 2. The assumptions for the heat exchangers off design calculation can be found in chapter 5.2while the most important simplification is a constant kA over the operating range. For the exhaust cooling diagram the low R2 and therefore high R1 are noticeable. The exhaust gas mass flow is much higher than the fuel mass flow which results in the large difference in enthalpie flows. Another interesting value

is the small dimensionless temperature difference P_i, while the difference for the exhaust flow is even lower. This is due to the low fuel flow in comparison to the exhaust mass flow. Therefore, the exhaust flow does not change its temperature for a high amount, see table 4. Other flight conditions lead to different heat transfer and therefore other NTU values. For higher loaded operating points, the achievable temperature change is lower. The huge difference in mass flow might lead to problems in further and more advanced heat exchanger designs since a large part of this mass flow might not take part in the heat transfer process. Higher loaded operating points, such as maximum take off, end of field and second segment, have lower P_i. Therefore, the outlet temperature is lower and the fuel temperature decreases.
The NTU values for the inter compressor cooling are similar to the values from the exhaust cooling. Just the P_i are sightly larger because maximal temperature difference between the flows is smaller. Since the absolute temperature difference is one of the main factors for heat transfer, to achieve the required fuel temperature in cruise fligt, a large heat exchanger is needed.
The cooled cooling air diagram differs from the other two due to the ratio of enthalpie flows R_i. For this concept, the R_i are closer to 1 because the enthalpie flows of the cooling air and the fuel are similar. This would lead to a completely different heat exchanger geometry for the CCA.

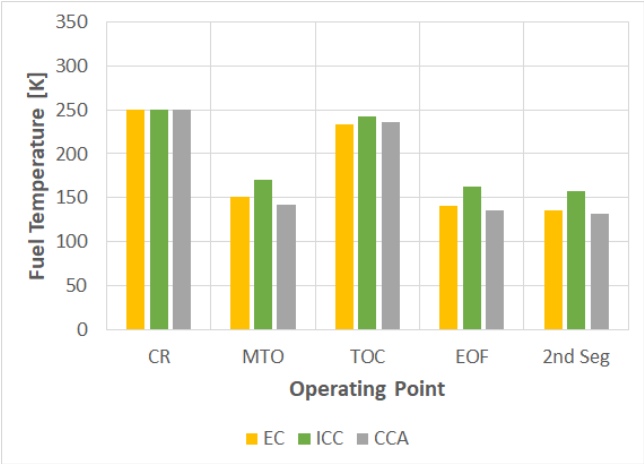

Figure 9 – Fuel temperature for different operating points

For each of the presented operating points, the fuel temperature leaving the heat exchanger is shown in figure 9. While the design temperature of 250 K is reached for all concepts in cruise flight, this temperature is different for other flight conditions. For points such as take off, temperatures within the engine and at the entry of the heat exchanger are generally higher. But so are the mass flows, the fuel to air ratios the pressure.

7. Conclusion and Outlook

This paper presents the thermodynamic potential of hydrogen combustion engines while considering the evaporation process of the liquid hydrogen for three different conditioning concepts. A maximum decrease in thrust specific energy consumption of 4.6 % is expected using inter compressor cooling. The other conditioning concepts lead to a decrease of 2.9 % for exhaust cooling and 1.7 % for cooled cooling air. The thrust requirements for a short range hydrogen driven airplane differs by a large amount in comparison to a standard kerosene application. Especially the required thrust at take off is about 11 % lower which results in a different loading at this rating. Hence, maximum take off might not be the design point for cooling air and might not be responsible for temperature limits. The higher water content of the exhaust flow leads to a higher specific enthalpy at turbine entry for the same temperature. Therefore, the engines core can extract more power from the air flow which results in a better thermodynamic cycle and less fuel consumption. While the fuels temperature is set at the design point, lower loaded operating points lead to higher fuel temperatures while higher loaded operating points lead to lower fuel temperatures. The acceptable range for this temperature is

not yet known. Whereas ICC provides the best thermodynamic potential, is also results in the largest and therefore heaviest heat exchanger. Using the heat exchanger data from this paper will assist the design process for such new components.

The off design behavior of the heat exchanger was simplified by calculating a kA for the cruise condition and keeping it constant throughout the operating range. This error increases the further the operating point is away from the design point. For additional calculation, this constant assumption should be replaced by another method considering differences in mass flow, temperature and pressure. The presented kA serves only as a measure for qualitative size evaluation. The real needed space and mass of the heat exchanger cannot be rated at this point. Methods of higher accuracy have to be implemented in the future. In addition, the boundaries for the fuel temperature are unclear looking at the combustion chamber, piping and the overall fuel system.

References

[1] Hasegawa T. Effects of Novel Coronavirus (Covid-19) on Civil Aviation: Economic Impact Analysis. 2021, Montreal. Available: https://www.icao.int/sustainability/Documents/Covid-19/ICAO_coronavirus_Econ_Impact.pdf

[2] Grewe V. Evaluating the climate impact of aviation emission scenarios towards the Paris agreement including COVID-19 effects. *Nature Communications*. 2021 https://doi.org/10.1038/s41467-021-24091-y.

[3] European Commission. Flightpath 2050 Europe's Vision for Aviation; Report of the Hight-Level Group on Aviation Research. *Luxembourg: Publications Office of the European Union*, 2011. https://data.europa.eu/doi/10.2777/50266

[4] Larsson L, Gronstedt T and Kyprianidis K G. Conceptual Design and Mission Analysis for a Geared Turbofan and an Open Rotor Configuration. *In Turbo Expo: Power for Land, Sea, and Air (Vol. 54617, pp. 359-370)*. 2011, https://doi.org/10.1115/GT2011-46451

[5] Gebisa A W and Lemu H G. Additive Manufacturing for the Manufacture of Gas Turbine Engine Components: Literature Review and Future Perspectives. *Turbo expo: Power for land, sea, and air, 51128, V006T24A021*, 2018. https://doi.org/10.1115/GT2018-76686

[6] Moxter T, Enders W, Kelm B, Scholjegerdes M, Koch C, Garbade M and Dahmann P. Investigation of Alternative Propulsion Concepts for Small Aircraft with the Hybrid Electric Motor Glider FVA 30. *Deutsche Gesellschaft für Luft-und Raumfahrt-Lilienthal-Oberth eV.*, 2021

[7] Seitz A, Nickl M, Troeltsch F and Ebner K. Initial Assessment of a Fuel Cell - Gas Turbine Hydrid Propulsion Concept. *Aerospace 2022, 9, 68*. https://doi.org/10.3390/aerospace9020068.

[8] Hoelzen J, Silberhorn D, Zill T, Bensmann B, and Hanke-Rauschenbach R. Hydrogen-powered aviation and its reliance on green hydrogen infrastructure–review and research gaps. *International Journal of Hydrogen Energy*, 2021. https://doi.org/10.1016/j.ijhydene.2021.10.239

[9] Haglind F and Singh R. Design of Aero Gas Turbines Using Hydrogen. *J. Eng. Gas Turbines Power. Oct 2006, 128(4): 754-764 (11 pages)*, 2006. doi:10.1115/1.2179468

[10] Brewer G D. *Hydrogen Aircraft Technology*. Routledge, 2017, nov, https://doi.org/10.1201/9780203751480

[11] Meyer P. Is there any available source of heat lighter than gasoline?. *NASA-TN-136*, 1923

[12] Westenberger A. Liquid hydrogen fuelled aircraft - system analysis. Final Technical Report (Publishable version). *GRD1-1999-10014, Submitted to the European Commission*, 2003

[13] Klug H G and Faass R. CRYOPLANE: Hydrogen Fuelled Aircraft - Status and Challenges. *Air & Space Europe*, Vol. 3, pp 252 - 254, 2001

[14] Price RO. Liquid hydrogen e an alternative aviation fuel. *Int J Hydrogen Energy 1991;16(8):557e62. Reprinted from Aerospace Engineering Magazine, Society of Automotive Engineers*, 1991

[15] Verstraete D. Long range transport aircraft using hydrogen fuel. *international journal of hydrogen energy*, 2013

[16] Wolters F, Becker R-G and Schaefer M. Impact of alternative fuels on engine performance and CO2 emissions. *28th International Congress of the Aeronautical Sciences (ICAS)*, Vol 23, 2012

[17] Grote K-H and Feldhuse J. *DUBBEL: Taschenbuch für den Maschinenbau*, Springer Berlin Heidelberg, 2005

[18] McCarty R D, Hord J and Roder H M. *Selected Properties of Hydrogen (Engineering Design Data)*, U.S. Department of Commerce, 1981

[19] Reitenbach S, Krumme A, Behendt T, Schnös M, Schmidt T, Hönig S, Mischke R and Mörland E. Design and application of a multidisciplinary predesign process for novel engine conceps. *Journal of Engineering for Gas Turbines and Power*, Vol 141, 2019

[20] Reitenbach S, Vieweg M, Becker R, Hollman C, Wolters F, Schmeink J, Otten T and Siggel M. Collaborative Aircraft Engine Preliminary Design using a Virtual Engine Platform Part A: Architechture and Methodology. *AIAA Scitech Forum. American Institute of Aeronautics and Astronautics*, 2020, doi:10.2514/6.2020-0867

[21] Becker R G, Wolters F, Nauroz M and Otten T. Development of a gas turbine performance code and its application to preliminary engine design. *DLRK 2011*, 2011

[22] German Aerospace Center (DLR), Simulation and Software Technology, Intelligent and Distributed Systems. Remote Component Environment, *https://rcenvironment.de/*, 2020

[23] German Aerospace Center (DLR), Institute of System Architecture in Aeronautics. Common Parametric Aircraft Configuration Schema. *https://cpacs.de*, 2018

[24] Alder M, Moerland E and Jepsen J. Recent advances in establishing a common language for aircraft design with CPACS. *Aerospace Europe Conference, Bordeaux*, 2020

[25] Woehler S, Atanasov G, Silberhorn D, Froehler B and Zill T. Preliminary Aircraft Design within a Multidisciplinary and Multi-fidelity Design Environment. *Aerospace Europe Conference, Bordeaux*, 2020

[26] Froehler B, Hesse C, Atanasov G and Wassink P. Disciplinary Sub-Processes to Assess Low-Speed Performance and Noise Characteristics within an Aircraft Design Environment. *Deutsche Gesellschaft für Luft-und Raumfahrt-Lilienthal-Oberth eV*, 2021

[27] Silberhorn D. AMC – Aircraft Mission Calculator Documentation. 2020

[28] Burschky T, Cabac Y, Silberhorn D, Boden B and Nagel B. Liquid hydrogen storage design trades for a short-range aircraft concept. *German Aerospace Congress, DLRK*, 2021

[29] Boeing Commercial Airplanes. 767 Airplane Characteristics for Airport Planning, D6-58328. *Boeing Commercial Airplanes Seattle, WA, USA*, 2021, https://www.boeing.com/resources/boeingdotcom/commercial/airports/acaps/767_REV_I.pdf

[30] Martin H, Gnielinski V, Mewes D, Stephan K, Schaber K and Kabelac S. VDI Heat Atlas. *VDI-Gesellschaft Verfahrenstechnick und Chemieingenierwesen. Springer*, 2010

[31] Söylemez M S. On the optimum heat exchanger sizing for heat recovery. *Energy conversion and management*, 2000. https://doi.org/10.1016/S0196-8904(99)00181-8

[32] Noie S H. Investigation of thermal performance on an air-to-air thermosyphon heat exchanger unsing ε-NTU method. *Applied Thermal Engineering*, 2006. https://doi.org/10.1016/j.applthermaleng.2005.07.012

[33] Gonser H. Untersuchung zum Einsatz von Wärmetauschern in zivilen Turboflugtriebwerken. *Institut für Luftfahrtantriebe der Universität Stuttgart*, 2008

[34] Piraino F, Blekhman D, Dray M and Fragiacomo P. Empirically verified analysis of dual pre-cooling system for hydrogen refuelling station. *Renewable energy*, 2021. https://doi.org/10.1016/j.renene.2020.10.004

[35] Silberhorn D, Dahlmann K, Görtz A, Linke F, Zanger J, Rauch B, Methling T, Janzer C and Hartmann J. Climate Impact Reduction Potentials Of Synthetic Kerosene and Green Hydrogen powered Mid-Range Aircraft Concepts. *Applied Sciences*, 2022

[36] Guha A. Optimum Fan Pressure Ratio for Bypass Engines with Separate or Mixed Exhaust Streams. *Journal of Propulsion and Power*, Vol. 17, 2001, pp. 1117-1122. doi:10.2514/2.5852.

[37] Grieb H. *Projektierung von Turboflugtriebwerken*. Springer, 2013

[38] Corchero G and Montanes J L. An approach to the use of hydrogen for commercial aircraft engines. *Proceedings of the Institution of Mechanical Engineers, Part G: Journal of Aerospace Engineering*, 2004. DOI: 10.1243/095441005X9139

Copyright Statement